An Acad Bras Cienc (2022) 94(Suppl. 3): e20210544 DOI 10.1590/0001-3765202220210544
Anais da Academia Brasileira de Ciências | *Annals of the Brazilian Academy of Sciences*
Printed ISSN 0001-3765 I Online ISSN 1678-2690
www.scielo.br/aabc | www.fb.com/aabcjournal

GEOSCIENCES

Geochemistry of a spheroidal weathering profile in a tropical mountainous landscape, Rio de Janeiro, Brazil

CARLA S. SILVEIRA, JULIANA G. RODRIGUES, DENISE R. ARARIPE, ALFREDO V.B. BERNEDO & JOSÉ L. MANTOVANO

Abstract: Boulders are an important material in debris flow and their source is coupled with spheroidal weathering profiles that produce corestones. The goal of this work was to establish the geochemical transformations that produced corestones and distinguished them from the surrounding grus in two tropical granite weathering profiles (P1 and P2). Sampling was not performed in a vertical profile; instead, we gathered 13 (P1) to 16 (P2) samples displaying different weathering degrees (corestone and saprolite) and spatial positions in the profiles. We conducted the geochemistry (EDXRF/EDX and INAA) and mineralogy (petrography and XRD) of the samples. The CIA values ranged from 46 (corestones) to 93 (saprolite). Granite spheroidal weathering under a tropical mountainous slope develops mostly due to feldspar weathering (foremost plagioclase) in the following sequence: porosity growth, kaolinite, and gibbsite crystallization. Zircon weathering stability and its probable mobility as grain along the weathering profile play an important role in REE concentration. Spheroidal weathering is mainly a lixiviation process, yet specific locations (below the individualized corestones) presented REE enrichment due to translocation. They are hosted mainly by clay minerals and, to some extent, by amorphous Fe oxyhydroxide. The evolution of spheroidal weathering results in a vertical patchy weathering profile.

Key words: corestone, feldspar, lixiviation, regolith, saprolite.

INTRODUCTION

The knowledge on weathering processes is essential, since these fundamental processes are responsible for the geomorphological evolution of landscapes (Stallard 1995, Turkington et al. 2005, Brantley et al. 2011, Hall et al. 2012) and environmental planning (Ehlen 2005). The difficulties to link different space and time scales resulted in a great variety in approaches towards studying weathering processes. They are based on natural processes measurements (hydrogeochemistry or regolith geochemistry in a watershed scale) as well as modeling proposals (Stallard 1985, Middelburg et al. 1988, Prudêncio et al. 1993, White et al. 1996, 1998, Nesbitt & Markovics 1997, Turner et al. 2003, Aide & Aide 2012).

Homogeneous rocks like basalts and even coarse-grained granite show spheroidal weathering processes during regolith generation. Spheroidal weathering is primarily defined as the process where rocks scale off in concentric shells, producing rounded boulder-like forms (Chapman & Greenfield 1949, Ollier 1971). When those rocks are well jointed, the corners of a boulder suffer attacks in all directions and, often, there is an abrupt physical change between the fresh rock (corestone) and the weathered rock, defined as the weathering front. This results

in a concentric shell surrounding a corestone. Around the '70s, Ollier (1971) had already pointed out that the term spheroidal weathering covered different features that probably formed in several different ways. Recent studies use spheroidal weathering to discuss geochemical processes (Babechuk et al. 2014, Banerjee et al. 2016, Banerjee & Chakrabarti 2018), landscape evolution (Fletcher et al. 2006, Lebedeva et al. 2007, Brantley et al. 2011), or weathering rates calculation (Chabaux et al. 2013, Behrens et al. 2015).

The coupling of chemical and physical processes in spheroidal weathering enhances the weathering rate. It also promotes a "patchy" distribution of weathering products because corestones and the grus material (saprolite) have different physical rock properties (Royne et al. 2008). During rainfall, these weathering discontinuities act as waterflow discontinuities that can led to slope failure (Wen et al. 2004, Shuzui 2001, Borrelli et al. 2014).

During the Mega Disaster of January 11 – 12, 2011, heavy rainfall and thunderstorms triggered thousands of landslides and debris flows along many small catchments in the mountainous region of Rio de Janeiro. Nearly 1,000 people died (Banco Mundial 2012). Debris flow happened simultaneously in many valleys. Boulders and sand constituted the main erosion material (Coelho Netto et al. 2011, Avelar et al. 2011, Rodrigues et al. 2013, Fraifeld & Freitas 2013, Conq et al. 2015, Cardoso & Vieira 2016, Gonçalves & Francisco 2016). After the disaster, during field excursions in the headwaters of one of these valleys, it was observed that the granite weathering profiles exposed due to the landslides presented spheroidal weathering features that could explain the source of the debris flows boulders. To understand the geochemical transformations that distinguished the corestones from the surrounding grus, we performed detailed sampling and analysis of two granite weathering profiles.

MATERIALS AND METHODS

Study site

The study area is located in the headwaters of the Principe catchment. The Principe catchment is a third-order watershed NW-SE oriented and with a 12 km^2 area. A big debris flow of 3.6 km long and between 40 m and 180 m wide destroyed 42% of the houses (Conq et al. 2015). This catchment is one of the headwaters of the Paraíba do Sul River Basin. This is the most important drainage system in southeast Brazil (Figure 1). The slopes are steep, and the valley is filled with silty clay colluvium alluvium, rich in blocks. The soil is classified as Cambisol. The annual rainfall is 2,300 mm (Marques et al. 2017). The climate is moderate mesothermal, humid to super–humid, with an average temperature of 18°C. The dry season is the winter (mainly July and August) and the wet season is summer. January is the rainiest month, with an average rainfall of 240 mm (Marques et al. 2017). However, it rained 270 mm between January 11 and 12, 2011, (Coelho Netto et al. 2011, Valverde & Marengo 2014).

The study area belongs to the Ribeira Belt (Oriental tectonostratigraphic terrane). The geology of the watershed is characterized by gneisses cut by two elongated intrusive bodies, of fine oriented biotite monzogranite (Teresópolis Granite) (Heilbron et al. 2017). The granite bodies are located in the watershed headwaters, where this study was performed.

Sample collection

We chose two granite weathering profiles (named P1 and P2) with spheroidal weathering features. The location of both profiles (near each other about 500 m) were in the headwater of the Principe catchment and they were exposed

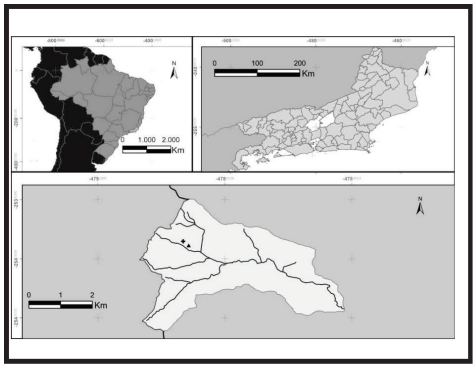

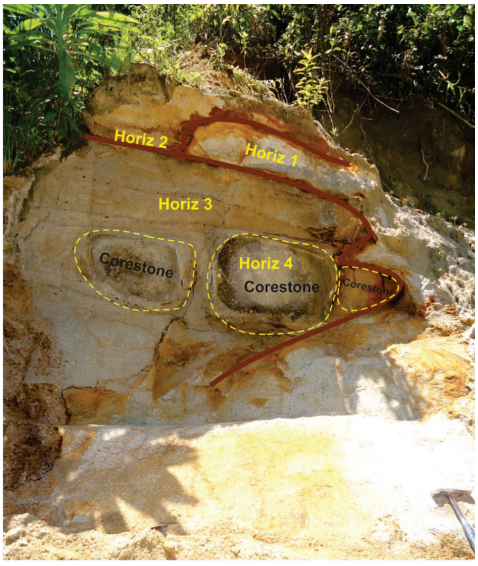

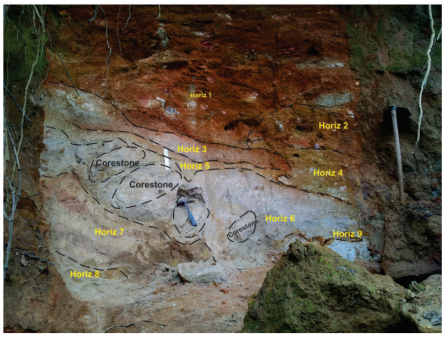

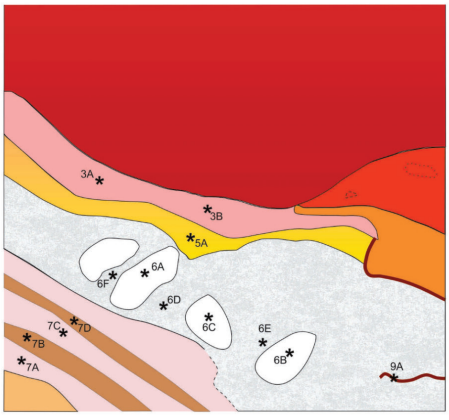

1 m

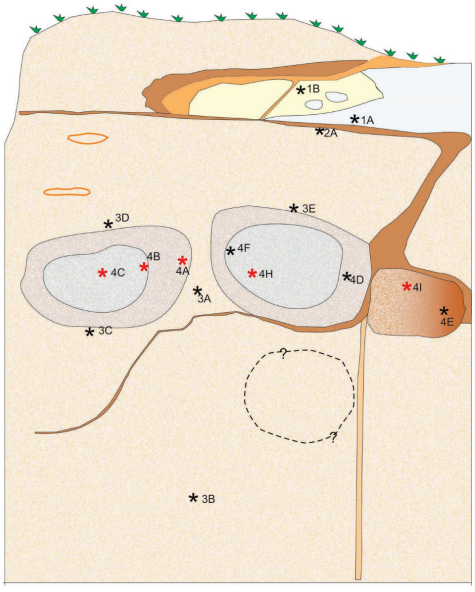

1 m

Figure 1. **Above location of profiles 1 (triangle) and 2 (cross) in Principe Catchment, Rio de Janeiro State, Brazil. Below photos and sketch of profiles 1 (left) and 2 (right) with horizons, corestones boundaries position (?: sugestion) and samples location. Samples 5A, 6A, 6B, 6C, 6D, 6E, 6F, 7A, 7B, 7C, 7D, 9A (profile 1) and 1A, 1B, 2A, 3A, 3B, 3C, 3D, 3E, 4A, 4B, 4C, 4D, 4E, 4F, 4H, 4I (profile 2) are described in Table I.**

due to the landslide's scars from the 2011 Mega Disaster. P1 was 3 x 3 m and P2 was 2x2 m. We scrapped the profiles before sampling and did a field description. At the time of sampling, we assessed the weathering degree, based on physical appearance. We did not sample in a vertical profile; we instead gathered 13 (P1) to 16 (P2) samples with different weathering degrees and spatial positions from the corestones observed in the profiles (Figure 1). Corestones were around 50 cm diameter and 50 cm apart from each other. The kilogram-size samples were classified according to their physical appearance and properties as corestones material (CR) - the hardest isolated blocks or boulders which, from the field point of view, seemed to be closer to a fresh rock; and saprolite material (SA). The term saprolite is used here as a synonym for grus, or "the sandy weathering product of granite formed by physical disintegration" (Ehlen 2005). The sampling was more intensive closer

to the spheroidal weathered zone around the corestones.

Pre-treatment of the samples and analytical methods

We ground the corestone and saprolite samples in a Mier/Mill 80000 with tungsten carbide balls and separated the silt-clay fraction (< 63 µm) from the saprolite samples. Mineralogy was carried out through X-Ray Diffraction (XRD) (Bruker D8 from Universidade Federal Fluminense - UFF, with CuK source; samples were read in 3^{o} – 70^{o}, 0.3s, and 0.02^{o} step) and identified through PCW and EVA software using PDF tables. The petrographic analysis of the thin sections from the corestones and observation of the sand fraction with a binocular loupe (Zeiss – Stemi 2000-C - UFF) from the saprolite samples improved the mineralogical analysis.

We analyzed the bulk compositions of the ground samples with EDXRF/EDX (800HS, Shimadzu Si (Li) detector; 50KV and 1000µ) at the Nuclear Engineering Institute of Rio de Janeiro /IEN-RJ) for Si and Ca. We used Instrumental Neutron Activation Analysis (INAA) Al, Mg, K, Na, Fe, Ti, Mn, U, V, Sc, Co, Rb, Sb, Cs, Hf, Ta, Th, Ba, Cr, La, Ce, Sm, Eu, Yb, Dy, Lu. San Joaquin Soil, Granite G-2 (USGS), with Red-Clay PODMORE (produced by the University of Manchester, (Araripe et al. 2011) used as standards. For each sample and standard, we weighted and irradiated around 200 mg at the AIEA-R1 reactor of the Institute of Nuclear Energy and Research (IPEN) ($10^{13} cm^{-2}.s^{-1}$ neutron flux). We counted the irradiated samples in ORTEC´s high purity Ge detector (GeHP), and also in CAMBERRA´s low energy photon detector (GAMX). The resolution for the 1332.5 keV gamma-ray of ^{60}Co was 2.8 keV and 1.8 keV, respectively. We used the same geometry for samples and standards. Irradiation time and counting time were, respectively, 5 seconds and 4 minutes for short-lived radionuclides, 90 s and 5 hours for intermediate-lived radionuclides, 2 hours and 2 hours (after a month of cooling time) for the long-lived radionuclides. We analyzed the gamma spectra with the GRGAN code. This software allowed us to choose the background of each photopeak to be free of interferences (Bellido & Arezzo 1986). We converted the spectra collected with the Canberra program (Genie2k) to a CHN format for the GRGAN software.

We also measured the Loss of Ignition (LOI) and the geochemical data sum showed an average of 96.72 % (SD = 3.69). The results from duplicate analysis (seven samples) suggest an uncertainty of up to 10 %.

We used the multivariate statistical software package Statistica 8.0@ to perform descriptive statistics, cluster, and principal component analysis.

RESULTS AND DISCUSSION

We named the samples according to the horizon and profile they belonged to, as well as their physical behavior. For example, CR 6A-1 and CR 6B-1 are both samples from corestones taken from horizon 6 from profile 1) and SA 3A-1 and SA 3B-1 are both saprolite (grus material) taken from horizon 3 from profile 1. A brief description of the horizons, an indication of samples, and weathering intensity, calculated by CIA (Chemical Index of Alteration) (Nesbitt & Young 1982) is in Table I. The profiles with sample location are in Figure 1 and the geochemical data in Table II.

Geochemical classification

To classify the weathering intensity, we used CIA values (Nesbitt & Young 1982). Profile 1 has the most weathered samples (higher CIA values). Actually, even the samples inside the corestones show high CIA values (60-68). The CIA range goes up to 93. On the other hand, in profile 2, CIA values range between 46 inside the corestones to 79 in

Table I. Field description of horizons from profiles 1 and 2, samples taken and CIA values.

Profile 1			
Horizon	**Description**	**Samples**	**CIA value**
1	red colluvium with blocks	No sample	-
2	brown colluvium with blocks	No sample	-
3	Rose homogeneous material with very weathered rock fragments and 30 cm thickness. It seems to happen a translocation process between the horizon above. Transition with horizon 5 is gradual	SA 3A-1 SA 3B-1	80 80
4	light brown colluvium. Transition with horizons 5 and 6 is very steep / abrupt	No sample	-
5	Pale yellow leucocratic homogeneous material with 25 cm thickness	SA 5A-1	69
6	Gray friable horizon with 1.2 m thickness. Corestones are embedded in a very weathered material. Transition with horizons 7 and 9 are very steep / abrupt	CR 6A-1 CR 6B-1 CR 6C-1 SA 6D-1 SA 6E-1 SA 6F-1	68 65 60 70 74 68
7	Friable banded horizon (0.8 m thickness). Intercalation of leucocratic and melanocratic layers	SA 7A-1 SA 7B-1 SA 7C-1 SA 7D-1	88 88 89 93
8	Friable brown horizon, below horizon 7. Steep transition with horizon 7	No sample	-
9	Milimetric brown horizon with oxide material	SA 9A-1	80
Profile 2			
Horizon	**Description**	**Sample**	**CIA value**
1	White gray horizon with 0.4 m thickness. It seems like “phantom corestones” are embedded in a very weathered material. Transition with horizon 2 is very steep / abrupt and it lets a brown material percolation	SA 1A-2 SA 1B-2	64 61
2	Milimetric to centrimetric hard brown horizon. Transition with neighbourhood horizons is very abrupt although it lets a brown material percolation.	SA 2A-2	62
3	Pale rose friable horizon with 2,0 m thickness. The steep / abrupt transition with horizon 4 is due to hardness difference	SA 3A-2 SA 3B-2 SA 3C-2 SA 3D-2 SA 3E-2	79 58 68 64 58
4	Gray material horizon about 0,5 m thickness made of corestones. Samples were taken along the concentric shells from the spheroidal weathering and inside the corestones	CR 4A-2 CR 4B-2 CR 4C-2 CR 4D-2 CR 4E-2 CR 4F-2 CR 4H-2 CR 4I-2	64 56 53 55 47 46 55 52

Table II. Geochemical data of the samples.

		(%)									mg/kg																		
Sample	CIA	LOI	SiO2	Al2O3	K2O	Fe2O3	MgO	Na2O	CaO	TiO2	Ba	Rb	Mn	Cr	Co	V	Cs	Sc	Sb	La	Ce	Sm	Eu	Dy	Yb	Lu	Th	U	Hf	Ta
							x10^{-1}	___ x 10^{-2}_____											x 10^{-2}							x 10^{-2}			
SA3A-1*	80	8.81	45.7	24.2	4.94	5.09	17.8	18.0	13.0	56.0	609	321	261	18.0	10.8	20.9	8.40	10.3	5.00	155	449	22.5	2.20	7.40	2.66	5.00	67.1	11.2	28.2	2.35
SA3B-1	80	8.94	47.5	22.3	4.83	5.29	13.9	17.0	5.00	78.0	441	302	312	20.5	12.4	17.4	8.17	12.8	5.00	172	465	22.4	1.63	6.91	3.33	5.00	67.3	11.0	26.0	2.16
SA5A-1*	69	5.75	58.5	16.0	6.19	4.33	7.80	24.0	7.00	51.0	581	290	182	14.9	11.7	16.0	6.75	9.30	4.00	174	386	22.6	2.11	5.59	2.00	4.00	58.8	11.7	23.0	2.20
CR6A-1	68	4.74	59.7	17.2	6.89	3.24	11.2	28.0	8.00	36.0	438	465	213	21.0	25.7	7.03	6.85	6.93	3.00	118	491	17.2	2.32	3.67	1.52	4.00	86.2	9.93	26.8	1.82
CR6B-1	65	5.40	57.5	17.8	8.22	2.92	11.1	40.0	10.0	32.0	570	542	155	33.3	70.2	6.18	7.06	7.17	4.00	102	456	12.3	3.00	6.11	2.18	2.00	79.0	10.2	23.5	1.25
CR6C-1	60	5.69	57.0	18.1	10.5	3.07	11.0	42.0	8.00	32.0	397	440	189	90.0x10^{-3}	78.9	6.99	6.52	6.78	3.00	154	386	25.1	2.27	6.02	1.97	3.00	66.7	13.0	21.1	1.23
SA6D-1	70	6.34	58.2	18.8	7.03	3.70	12.0	32.0	6.00	41.0	441	372	186	30.0x10^{-3}	17.6	12.9	6.31	8.09	3.00	155	426	13.7	2.41	4.24	1.56	1.00	64.5	11.9	22.6	1.44
SA6E-1	74	7.24	52.1	22.2	6.62	3.85	12.8	27.0	6.00	45.0	392	342	228	18.3	11.1	13.2	6.76	9.76	3.00	207	498	22.6	2.43	7.75	2.21	3.00	74.5	11.7	21.8	1.54
SA6F-1	68	6.30	54.9	19.7	7.91	3.50	11.8	31.0	11.0	43.0	285	288	195	30.0x10^{-3}	10.5	10.7	6.06	7.41	3.00	199	409	26.3	2.19	5.61	1.23	2.00	60.2	14.2	20.1	1.31
SA7A-1	88	7.74	57.0	23.1	2.64	3.31	11.9	6.00	2.00	47.0	494	185	217	14.5	12.1	7.58	8.04	9.21	4.00	237	463	28.7	2.88	8.73	2.85	4.00	47.1	13.7	17.0	1.56
SA7B-1	88	7.38	58.7	18.6	2.10	4.16	16.9	7.00	2.00	53.0	529	204	605	21.6	23.2	14.6	9.73	9.94	5.00	174	503	26.0	2.53	5.41	2.94	5.00	60.7	12.3	21.1	1.72
SA7C-1	89	8.07	53.5	23.5	2.50	3.60	12.9	6.00	2.00	49.0	417	188	163	10.8	14.8	29.9	7.31	9.53	3.00	187	408	21.5	3.03	7.44	3.07	4.00	45.3	10.5	18.0	1.47
SA7D-1*	93	9.20	51.1	26.7	1.78	3.58	15.0	6.00	1.00	47.0	617	113	532	18.1	15.3	12.7	6.89	8.54	4.00	219	428	30.8	2.31	8.44	2.35	5.00	53.9	16.0	18.8	6.20x10^{1}
SA9A-1*	80	8.48	46.5	24.5	5.13	8.61	17.4	21.0	6.00	56.0	401	246	845	45.2	28.2	38.7	4.63	17.0	3.00	123	577	18.1	1.57	5.47	1.57	4.00	48.6	9.04	15.0	1.09
SA1A-2	64	4.66	59.9	16.6	7.99	3.84	8.50	34.0	10.0	54.0	191x10^{1}	481	305	8.02	11.5	22.8	15.5	10.7	8.00	458	895	46.6	6.60	1.27	8.35	107	105	23.9	26.1	3.16
SA1B-2	61	3.51	63.8	19.6	10.4	1.13	12.6	57.0	11.0	28.0	794	414	172	25.4	8.44	9.09	13.0	5.26	7.00	184	593	19.6	2.73	7.33	4.60	7.00	73.2	9.08	13.5	3.78
SA2A-2*	62	7.42	36.2	12.6	6.40	34.6	8.80	28.0	10.0	48.0	135x10^{1}	266	346x10^{1}	19.3	52.2	74.7	8.90	7.66	5.00	377	712	46.8	5.30	15.5	8.00	8.00	48.2	23.5	18.3	1.72
SA3A-2	79	6.10	51.9	31.0	6.10	6.42	23.2	67.0	38.0	98.0	533	379	747	114	21.5	102	17.2	13.6	8.00	204	406	18.1	2.64	8.97	4.27	7.00	66.7	6.98	21.6	2.84
SA3B-2*	58	3.01	62.4	15.3	9.02	4.00	11.8	68.0	15.0	25.0	389	444	216	18.7	15.3	10.7	10.1	4.95	5.00	112	328	15.9	1.85	3.72	2.16	4.00	47.3	6.59	17.9	1.75
SA3C-2	68	4.16	57.9	18.4	7.04	5.77	14.7	44.0	21.0	67.0	129x10^{1}	492	501	39.0	18.8	40.2	10.2	8.77	5.00	409	106x10^{1}	38.2	7.57	16.5	11.4	178	137	19.7	35.3	3.85
SA3D-2*	64	3.74	60.9	18.7	8.46	4.45	13.0	54.0	16.0	43.0	696	381	409	15.0	15.8	31.0	6.13	6.67	3.00	236	634	25.6	4.20	9.43	5.91	60.0	97.5	12.7	25.2	2.60
SA3E-2	58	3.56	60.8	14.5	8.70	2.76	8.90	42.0	14.0	67.0	835	250	275	30.0x10^{-3}	7.64	31.3	4.55	4.16	2.00	310	350	32.6	3.31	10.0	4.27	4.00	42.8	16.0	15.3	1.82
CR4A-2	64	3.21	60.1	19.0	6.69	2.84	15.1	139	73.0	67.0	361	332	296	15.2	17.8	29.2	7.07	3.98	3.00	86.2	403	7.82	2.80	3.71	1.38	3.00	68.1	6.54	24.7	1.14
CR4B-2	56	1.70	63.3	17.7	6.87	4.03	10.3	244	146	34.0	965	367	265	30.0x10^{-3}	19.0	22.8	5.21	6.52	2.00	243	839	20.4	5.27	10.6	6.10	8.00	110	12.9	32.0	2.54
CR4C-2	53	1.69	63.2	17.2	7.39	3.64	8.20	275	158	47.0	992	362	247	33.2	11.2	21.7	5.10	5.89	3.00	286	732	31.3	5.54	10.3	6.70	103	127	15.0	31.5	2.47
CR4D-2	55	3.99	59.1	13.4	8.89	5.60	10.9	51.0	17.0	42.0	393	507	767	30.0x10^{-3}	10.7	25.3	10.1	8.30	5.00	118	240	11.4	3.02	8.48	5.90	9.00	126	6.18	39.2	4.75
CR4E-2	47	2.88	58.9	12.0	9.65	12.4	9.50	138	53.0	58.0	559	488	545	26.6	25.9	62.9	6.51	10.1	3.00	176	595	21.1	4.28	8.00	5.98	8.00	155	8.45	41.0	4.64
CR4F-2	46	1.23	64.2	14.6	8.77	3.72	12.3	280	152	50.0	650	319	315	40.0x10^{-3}	10.0	34.3	5.13	6.16	2.00	278	476	27.9	5.23	11.6	5.94	7.00	82.9	12.8	26.8	2.75
CR4H-2	55	7.93x10^{-1}	65.4	20.2	7.63	4.39	10.9	258	171	77.0	979	362	392	40.0x10^{-3}	11.9	38.3	5.64	6.82	3.00	376	694	31.1	7.19	22.1	9.62	119	85.5	14.9	27.2	2.49
CR4I-2	52	1.31	64.1	17.0	7.90	4.80	9.80	297	157	81.0	686	405	277	18.6	12.5	31.1	5.85	7.68	3.00	243	813	25.5	5.50	7.71	5.88	103	154	14.3	41.2	4.35
* duplicate samples																														

the saprolite samples. The Al_2O_3- K_2O - Na_2O+CaO triangular diagram (Figure 2) indicates two main weathering pathways, from inside to outside the corestones. First, there is a Na_2O+CaO loss. This process happens "very quickly" because it doesn't leave many remnants. The samples from profile 2, on the border of the corestones (CR4E-2, CR4A-2, and CR4D-2), have almost no Na_2O and CaO compared to those inside them (CR4C-2, CR4H-2, CR4I-2) or next to its center (CR4B-2, CR4F-2).

The next step is a shift towards the continuous loss of K_2O. We plotted, along with this second trend, all the samples from profile 1 (even the corestones). Nesbitt et al. (1980), in an Australian granodiorite, also pointed out that the bulk of Na and Ca is leached during early and intermediate stages of weathering compared to K.

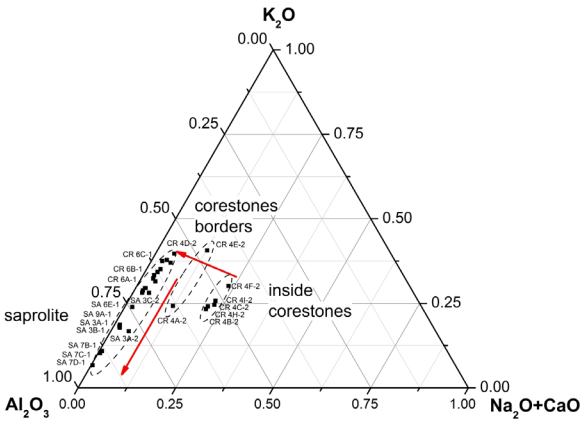

Figure 2. Al_2O_3 – CaO+ Na_2O – K_2O diagram with plotted samples. Arrows show first a trend towards loss of CaO+ Na_2O and then a continuous loss of K_2O together with a relative enrichment of Al_2O_3 from corestones to saprolite samples.

Statistical geochemical approach

We performed a PCA multicomponent analysis using all the geochemical data from both profiles (Table III). The threshold value for the factors in the multivariate analysis was 0.5. Factors 1 and 2 together explain almost 51% of the sample's variance.

Considering the two key factors, the results showed mainly 3 groups and 3 outliers (Figure 3). The first group contains the samples from inside the corestones from profile 2 (CR4B-2, CR 4C-2, CR4E-2, CR4F-2, CR 4H-2, and CR 4I-2). The second group contains both corestones (CR 4A-2, CR 4D-2, CR 6A-1, CR 6B-1, CR 6C-1) and saprolite samples (SA 1B-2, SA 3B-2, SA 3D-2, SA 3E-2, SA 5A-1, SA 6D-1, SA 6E-1, SA 6F-1). Group 3 contains only saprolite samples (SA 3A-1, SA 3B-1, SA 7A-1, SA 7B-1, SA 7C-1, SA 7D-1, SA 9A-1, SA 3A-2). The three outliers are SA 1A-2, SA 2A-2, and SA 3C-2, all located below corestones.

Group 1 has the rock samples with the highest concentration of Na_2O, CaO, Th, Hf, and Ta. They are the freshest rocks, with CIA values from 46 to 56. High concentrations of other elements such as La, Ce, Eu, Dy, Yb, and Lu are also associated with rock samples from this group. Group 2 samples have an intermediate behavior between groups 1 and 3. They are a gradation process (CIA values between 55 and 74), a trendline parallel to factor 1. So, they show a continuous loss of the abundant elements from group 1, with increasing LOI values. Those samples are from the borders of corestones or the smaller sizes corestones from profile 1.

From group 2 to group 3, there is a shift towards a positive factor 2, which means a continuous loss of SiO_2 along with an increase in Fe_2O_3, MnO, Sc, V, Sm, U, Sb, and LOI. They are all saprolite samples with CIA values greater than 79. LOI reflects the increase in the amount of clay minerals. For Fe_2O_3, MnO, there are stable phases (oxide or hydroxide) and, under high redox potential, U and V make compounds with low solubility. The absorption on ferric hydroxide by Sb causes its enrichment (Middelburg et al. 1988, Murakami et al. 1997, Takeno 2005). Although Sc is a trace element, it plays an important role as it substitutes Al and

Table III. Factors from multivariate analysis.

	Factor 1 (31,5 %)	Factor 2 (19,2%)	Factor 3 (12,7%)	Factor 4 (9.2%)
SiO_2	-0.41	**-0.74**	-0.17	0.10
Al_2O_3	0.49	0.41	-0.40	0.47
K_2O	-0.43	-0.48	-0.07	**-0.52**
Fe_2O_3	-0.20	**0.59**	0.31	-0.30
MgO	0.46	0.39	**-0.60**	0.25
Na_2O	**-0.66**	-0.41	-0.13	0.38
CaO	**-0.65**	-0.34	-0.11	0.47
TiO_2	-0.24	0.41	-0.49	0.45
Ba	**-0.75**	0.43	0.19	-0.16
Rb	-0.43	-0.36	-0.38	**-0.64**
Mn	-0.16	**0.65**	0.30	-0.27
Cr	0.12	0.48	**-0.70**	-0.03
Co	0.13	0.08	0.22	-0.47
V	-0.31	**0.55**	-0.38	0.01
Cs	-0.02	0.48	**-0.53**	-0.46
Sc	0.28	**0.58**	-0.39	0.09
Sb	-0.01	**0.50**	-0.48	-0.46
La	**-0.76**	0.47	0.26	0.13
Ce	**-0.78**	0.27	0.00	0.06
Sm	**-0.55**	**0.59**	0.45	0.04
Eu	**-0.96**	0.13	0.06	0.11
Dy	**-0.58**	0.26	0.12	0.35
Yb	**-0.92**	0.28	-0.06	-0.01
Lu	**-0.80**	0.13	-0.14	0.16
Th	**-0.74**	-0.28	-0.38	-0.12
U	**-0.55**	**0.50**	**0.55**	0.01
Hf	**-0.62**	-0.29	-0.37	-0.03
Ta	**-0.65**	-0.12	**-0.50**	-0.26
LOI	**0.72**	**0.57**	0.13	-0.01

Fe in hydroxides in soils of residual deposits (Bowen 1982). It is one of the least mobile trace elements in a weathering profile, therefore we chose it in the element-mass-transfer analysis (section Rindlets geochemical transects).

The correlation between MgO, Cs, and Cr in factor 3 indicates their possible association to micas. The elements Mg, K, Ba, Rb, and Cs have a dual behavior as they could be transported both in solution as well as constituents of clays (Nesbitt et al. 1980). The confirmation of the behavior is due to both factors 1 and 2 weakly explain them.

Although the concentrations of La, Ce, Eu, Dy, Yb, Lu, and mostly Sm and U presented high values in the Group 1 samples, the outliers showed even higher values. Therefore, the outliers indicate different geochemical

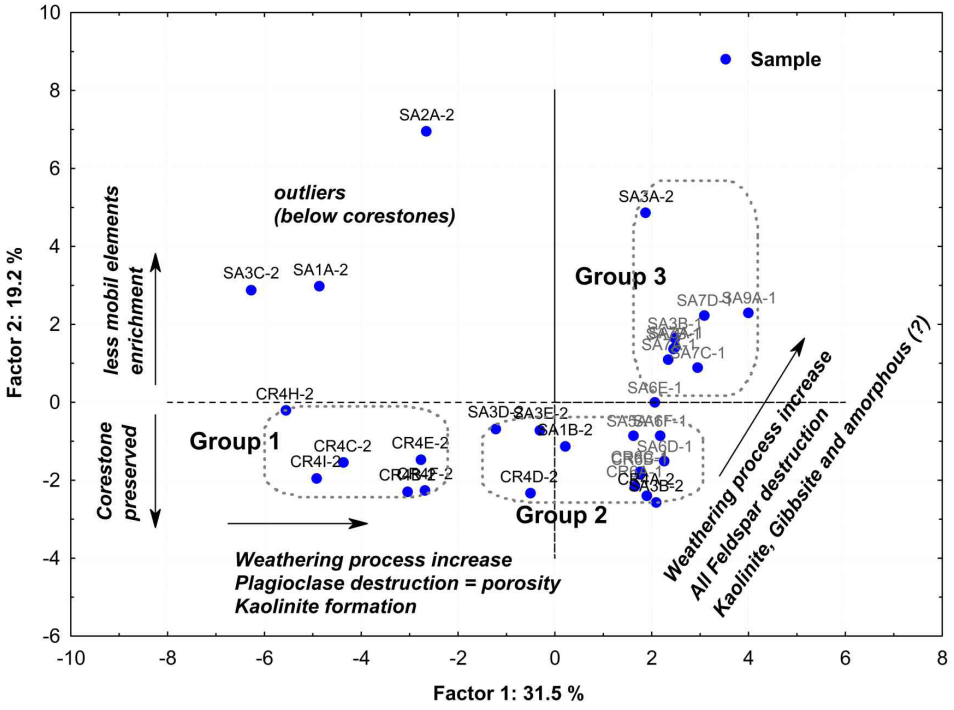

Figure 3. Principal Component Analysis (PCA) diagram from factors 1 and 2 per cases (samples).

processes from the whole weathering profile. The enrichment of both Ba, La, Ce, Eu, Yb, and more immobile elements such as Fe, Sm, and U characterizes those samples (SA 1A-2, SA 2A-2, and SA 3C-2).

Sample SA 3A-2 is a different kind of outlier, as it is apart from the other ones on Group 3. Its spatial position between 2 large corestones represents a region of higher water flow percolation. This could have caused a higher lixiviation process, in a way that this sample represents a very depleted corestone boundary case.

In summary, the negative factor 1 is also defined by a high concentration of REE and similar elements (Th, Hf, Ta, Ce, Yb, Lu, Eu, La, and Dy) that are present in the fresh rock. Factor 2 is both due to elements' mobility in an oxidizing environment and the physical condition of the samples (corestone or saprolite). The negative value is associated with the corestone samples. The positive factor 2 is due to a relative enrichment of less mobile elements such as Al, Mn, Fe, U, and Sm under high oxidoreduction potential. Thus, we could describe (except for the outliers) factor 1 as a weathering index and factor 2 as a laterization process, such as defined by Babechuk et al. (2014).

Petrography and mineralogy

Rocks from group 1 are all corestones. We described them macroscopically as little or no weathered holocrystalline, equigranular, leucocratic, and not foliated. In thin sections, quartz and microcline are dominant. Plagioclase is around 10% and is sometimes partially weathered originating porosity, relict grains, and traces of a clay mineral (XRD showed that it is kaolinite). The samples show the dissemination of biotite. In some samples, a brown material - probably an amorphous iron composition, is inside the porosity having its source from biotite weathering. Zircon and opaque minerals are accessory minerals.

The rocks from group 2 are both corestones and saprolite samples. The main mineralogy

is quartz and microcline, although microcline crystals often show a weathering product (kaolinite or gibbsite) above them. Plagioclase grains are neither in thin sections nor in the XRD present. However, there is a great porosity (higher than group 1). Biotite is golden colored, suggesting the change to vermiculite. Kaolinite is widespread mainly in the silt clay fraction of the saprolite samples, and gibbsite also occurs in some samples. Microcline is more abundant in the bulk samples than in the silt clay fraction. That means microcline is more present in rock fragments than in saprolite. We also described hydrobiotite, a regularly interstratified biotite-vermiculite, formed as the result of the weathering path of biotite to vermiculite (Velde & Meunier 2008) in the group 2 samples.

Group 3 is composed only of saprolite samples. Quartz and biotite are the main composition of the primary mineralogy. XRD analysis shows the presence of gibbsite, kaolinite, and, in some samples, vermiculite, and hydrobiotite. Microcline occurs both in total and silt-clay fractions, in a small amount. Because of the high concentration values of Al, we suggest that part of it should be in an amorphous phase.

The three outliers are, mineralogically, composed mainly of quartz, microcline, mica (biotite/illite), scarce to no plagioclase, and variable amounts of kaolinite. Figure 4 presents the main mineralogical differences among the groups, with typical XRD results.

Rindlets geochemical transects

In order to understand and normalize the changes around a corestone we followed the idea of Anderson et al. (2002), Babechuk et al. (2014) and calculated the dimensionless element-mass-transfer coefficient (τ) according to equation 1:

$$\tau_{i,j} = \frac{\left(\frac{\left(C_{j,w}\right)}{\left(C_{j,p}\right)}\right)}{\left(\frac{\left(C_{i,w}\right)}{\left(C_{i,p}\right)}\right)} - 1$$

$C_{j,w}$= concentration of an element *j* in a weathered sample.

$C_{j,p}$= concentration of an element *j* in the parent rock.

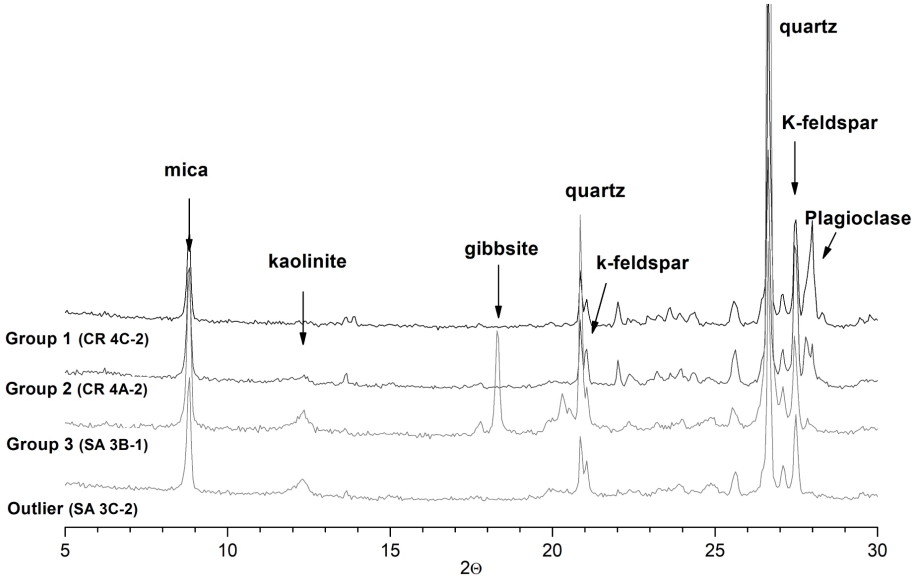

Figure 4. Typical XRD mineralogical results from samples from group 1 (CR 4C-2), group 2 (CR 4A-2), group 3 (SA 3B-1) and outlier (SA 3C-2).

$C_{i,w}$= concentration of the immobile element *i* in a weathered sample.

$C_{i,p}$=concentration of the immobile element *i* in the parent rock.

Sample CR4C-2, (inside a corestone, CIA=53) was chosen as parent rock and Sc as the immobile element. The $\tau_{Sc,j}$ values were calculated for 3 samples with increasing CIA values and nearby located in the weathering profile: a corestone border (CR4B-2, CIA value=56), below the corestone (SA3C-2 CIA value=68), and between 2 corestones (SA3A-2 CIA value=79) (Figure 5). According to mass gains (positive values) and losses (negative values) in the weathering process we classified the elements. The first ones are the classical continuous loss with CIA increment indicating that they are very susceptible to lixiviation processes moving away from corestones. They are Si, K, Na, Ca, Ba, Rb, Co, Ce, and (Eu), released mainly with feldspar weathering (plagioclase). Otherwise, in the second group Mn, Cr, V, Cs, and Sb show an enrichment with CIA increase (from inside through its border, below and between 2 corestones). Except for Cs that is strongly absorbed by clay minerals these elements have stable compounds dependent on pH and oxidoreduction potential (Takeno 2005). Therefore, their enrichment can be associated with oxidation processes. For Al, Fe, Mg, and Ti the normalization indicates little mobilization, close to Sc, neither enrichment nor loss.

La, Sm, (Eu), Dy and Yb, U, Hf, and Ta have a dual behavior between loss and gain. Under a high leaching environment, that is, between corestones, those elements are not present. However, they are enriched below the corestones. This location shift towards REE enrichment was more associated with clay minerals retaining (sample SA3C-2 has a great amount of illite and kaolinite) than with oxyhydroxide compounds (there is no correlation with Fe_2O_3, Sc, or Mn). At these locations, the lixiviation process acts together with a translocation process. So, there is a continuous gain from above, especially for REE together with loss from the more soluble elements.

Nesbitt & Markovics (1997) also showed that some REE (La, Eu, Sm) accumulated in the weathering profile at concentrations greater than those observed in fresh granodiorite. They proposed two zones for the weathering profile: the leaching and the accumulation zones. Since the latter was richer in REE, we understood the

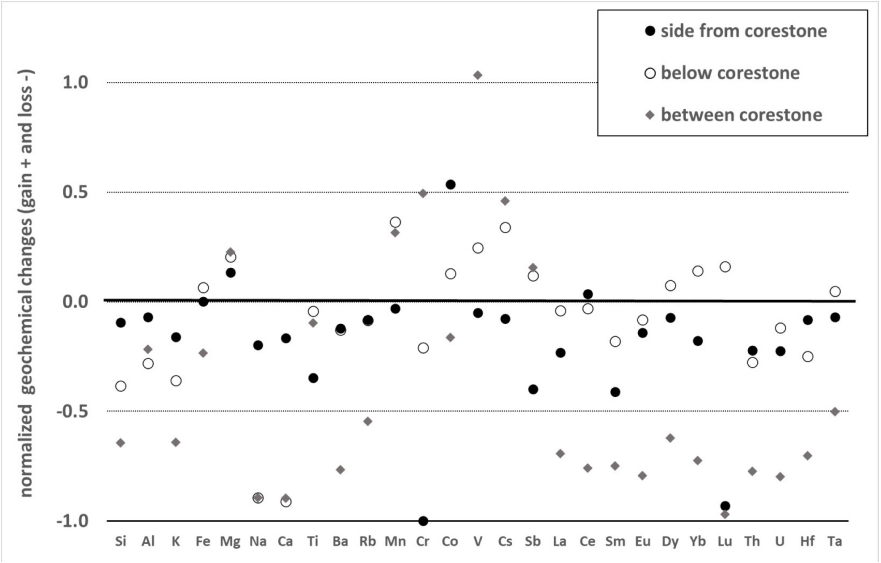

Figure 5. Normalized geochemical changes to show the gain (positive vales) and loss (negative values) from inside a corestone to its boundaries. Sample CR4C-2 (inside a corestone; CIA=53) was chosen as the parent rock and Sc as the immobile element. The samples from the side of the corestone, bellow and between corestones are respectively CR 4B-2 (CIA=56), SA 3C-2 (CIA=68) and SA 3A-2 (CIA=79).

location below the corestone (sample SA 3C-2) as a representative of the accumulation zone. On the other hand, between the corestones (sample SA 3A-2) is the furthest leaching process (leaching zone) being enriched with less mobile elements, probably in an amorphous phase, together with kaolinite, quartz, and a low amount of K feldspar, and illite.

DISCUSSION

In fresh rock, both zircon and feldspar host the REE. The former is a very stable mineral. However, it can be mobilized as grain along with the weathering profile (Colin et al. 1993, Balan et al. 2001, Aubert et al. 2001). So, considering Hf a tracer of zircon weathering, we recognize that, even in the most weathered samples, Yb, Lu, Th, Hf, and Ta are present indicating zircon grains as the source. The elements Ba, Na, Ca and Si make a strong and significant statistically correlation with La, Ce, Eu, Dy, Yb, Lu in the less weathered samples (lower CIA values, group 1 and 2 from section Statistical geochemical approach) that disappear as the weathering advances, indicating their source is feldspar (mainly plagioclase) weathering.

As feldspar is removed, REE remains attached to clay minerals (illite/hydrobiotite) (and locally in iron oxyhydroxides). For the more weathered and outlier samples, K has a statistically significant positive correlation ($p< 0.05$) to Eu (0.65), La (0.65), Ce (0.72), Yb (0.73), Lu (0.61), Ta (0.76), Th (0.64), indicating that illite/hydrobiotite hosts most of the REE removed from the weathering profile. A similar process with kaolinite was proposed by Yusoff et al. (2013) to explain the retaining of REE in the saprolite.

Early plagioclase weathering has also been noticed in other rocks such as diabase (Banerjee et al. 2016), gneiss and granite (Borrelli et al. 2014); granodiorite (Turner et al. 2003), and quartz diorite (White et al. 1998). Biotite and Plagioclase dissolution was also described in spheroidal weathering processes in Charnockites in Sri Lanka (Behrens et al. 2015). In our weathering profiles, Biotite is not dissolved but changed to hydrobiotite and vermiculite.

After plagioclase dissolution, K-Feldspar reacts to form kaolinite and gibbsite (continuous loss of K and relative enrichment of Al). The breakdown of K-feldspar with a concomitant loss of K is not homogeneous in all directions around the corestones. Samples from beside and above the corestones can be associated with the leaching zones proposed by Nesbitt & Markovics (1997), or the lateritisation process proposed by Babechuk et al. (2014). Feldspar weathering processes lead to a physical change from rigid rock to a grus material, due to porosity development and clay mineral growth.

However, below the corestones, a different weathering process happens. Both clay minerals and amorphous Fe oxyhydroxides host these high REE concentrations under the corestones. Gouveia et al. (1993) and Li et al. (2017) proposed a zone with maximum REE enrichment in the middle part of the weathering profile (from the lower B horizon to the upper C horizon) as the special places (outliers) in the weathering profile. So, we can understand that the location below corestones has different weathering paths as the result of the translocation process in the profile that promotes a concomitant decrease in K feldspar weathering and enrichment of REE.

Fe has a very unclear behavior along the weathering profiles studied. The adsorption of the REE on Fe oxyhydroxides is not linear along the weathering process as seen in other studies (Middelburg et al. 1988, Silva et al. 2018). Neither the less weathered, nor the most weathered samples show any significant correlation between Fe and REE (except Dy). But the 3

samples below corestones are the ones with the higher Fe together with La, Ce, Sm, Eu, Y, and U.

CONCLUSIONS

We have presented data on the geochemistry of two granite spheroidal weathering profiles under a tropical mountainous slope. The study has revealed that weathering process develops mostly due to feldspar weathering (foremost plagioclase and then K feldspar). Zircon weathering stability and its probable mobility as grain along the weathering profile are responsible for most of Yb, Lu, Th, Hf, and Ta concentrations in the whole profile. For La, Ce, Eu, Dy, Yb, Lu, the main source in feldspar weathering. With the removal of feldspar, REE remains attached to clay minerals (illite/hydrobiotite) and locally in iron oxyhydroxides.

The spheroidal weathering process begins with plagioclase dissolution and porosity formation. At this time, fresh rock is still a corestone. As the weathering process goes on, geochemical changes (mainly feldspar weathering to kaolinite and gibbsite) differentiate corestones from the surrounding grus, promoting the transformation of bedrock to saprolite. The process is not the same around the corestones. Si, K, Na, Ca, Ba, Rb, Co, Ce, and (Eu)), are very susceptible to lixiviation processes moving away from corestones. They are released mainly with feldspar weathering. For Mn, Cr, V, and Sb, a strong lixiviation process between corestones promotes their enrichment due to stable compounds formation under high redox potential. Cs remains in the profile, absorbed by clay minerals. The elements La, Sm, (Eu), Dy and Yb, U, Hf, and Ta have a dual behavior between loss and gain. Under a high leaching environment, that is, between corestones, they are removed. However, they are enriched below the corestones due to both clay minerals and oxide hydroxide compounds retention. Fe has a very unclear behavior along the weathering profiles studied. The adsorption of the REE on Fe oxyhydroxides is not linear along the weathering process.

The tropic granite spheroidal weathering process is mainly a lixiviation process. But the translocation from the above corestones promotes the retention of REE hosted mainly by clay minerals and to some extent by amorphous Fe oxyhydroxides. At these locations, K feldspar weathering is also slowed. So, the evolution of spheroidal weathering results in a vertical patchy weathering profile.

Acknowledgments

This work was supported by Fundação de Amparo à Pesquisa do Estado do Rio de Janeiro – FAPERJ, Brazil (research support grant E-26/111.387/2014), Coordenação de Aperfeiçoamento de Pessoal de Nível Superior – CAPES, Brazil, and Conselho Nacional de Desenvolvimento Científico e Tecnológico – CNPq, Brazil (scholarship to J.G.R). We are also grateful to the comments from the revisors and editor that improve the manuscript.

REFERENCES

AIDE MT & AIDE C. 2012. Rare Earth Elements: Their Importance in Understanding Soil Genesis. Int Sch Res 2012(11): 1-11. doi:10.5402/2012/783876.

ANDERSON SP, DIETRICH WE & BRIMHALL JR GH. 2002. Weathering profiles, mass-balance analysis, and rates of solute loss: linkages between weathering and erosion. Geol Soc Am Bull 114: 1143-1158.

ARARIPE DR, BELLIDO AVB, PATCHINEELAM SR, LATINI RM, BELLIDO LF & FÁVARO DIT. 2011. Trace and major elements in geological samples from Itingusssú River Basin, Sepetiba Bay, Rio de Janeiro. J Radioanal Nucl Chem 290: 381-389.

AUBERT D, STILLE P & PROBST A. 2001. REE fractionation during granite weathering and removal by waters and suspended loads: Sr and Nd isotopic evidence. Geochim Cosmochim Acta 65: 387-406.

AVELAR AS, COELHO NETTO AL, LACERDA WA, BECKER LB & MENDONÇA MB. 2011. Mechanisms of the recent catastrophic landslides in the moutainous range of the

Rio de Janeiro, Brazil. In: Margottini C, Canuti P & Sassa K (Eds), Landslide Science and Practice, vol. 4, Global Environmental Change, Kyoto, Springer, p. 265-270.

BABECHUK MG, WIDDOWSON M & KAMBER BS. 2014. Quantifying chemical weathering intensity and trace element release from two contrasting basalt profiles, Deccan Traps, India. Chem Geol 363: 56-75.

BALAN E, TROCELLIER P, JUPILLE J, FRITSCH E, MULLER JP & CALAS G. 2001. Surface chemistry of weathered zircons. Chem Geol 181: 13-22.

BANCO MUNDIAL. 2012. Avaliação de Perdas e Danos: Inundações e Deslizamentos na Região Serrana do Rio de Janeiro – Janeiro de 2011. 2012. <https://documents1.worldbank.org/curated/pt/260891468222895493/pdf/NonAsciiFileName0.pdf>.

BANERJEE A & CHAKRABARTI R. 2018. Large Ca stable isotopic ($\delta^{44/40}$Ca) variation in a hand-specimen sized spheroidally weathered diabase due to selective weathering of clinopyroxene and plagioclase. Chem Geol 483: 295-303.

BANERJEE A, CHAKRABARTI R & MANDAL S. 2016. Geochemical anatomy of a spheroidally weathered diabase. Chem Geol 440: 124-138.

BEHRENS R, BOUCHEZ J, SCHUESSLER JA, DULTZ S, HEWAWASAM T & BLANCKENBURG F. 2015. Mineralogical transformations set slow weathering rates in low-porosity metamorphic bedrock on mountain slopes in a tropical climate. Chem Geol 411: 283-298.

BELLIDO LF & AREZZO B. 1986. Nondestructive analysis of inorganic impurities in Brazilian coals by epithermal neutron activation. J Radioanal Nucl Chem 100: 21-29.

BORRELLI L, PERRI F, CRITELLI S & GULLÀ G. 2014. Characterization of granitoid and gneissic weathering profiles of the Mucone River basin (Calabria, southern Italy). Catena 113: 325-340.

BOWEN HJM. 1982. Environmental Chemistry. V. 2 Specialist Periodical Report/Royal Society of Chemistry, 279 p.

BRANTLEY SL, BUSS H, LEBEDEVA M, FLETCHER RC & MA L. 2011. Investigating the complex interface where bedrock transforms to regolith. Appl Geochem 26: S12-S15.

CARDOSO PS & VIEIRA R. 2016. O Megadesastre de Janeiro de 2011 na cidade de Nova Friburgo, Rio de Janeiro: aspectos históricos desde a colonização suíça e as condicionantes físicas. Investig Geogr 52: 47-70.

CHABAUX F, BLAES E, STILLE P, DI CHIARA ROUPERT R, PELT E, DOSSETO A, MA L, BUSS HL & BRANTLEY SL. 2013. Regolith formation rate from U-series nuclides: Implications from the study of a spheroidal weathering profile in the Rio Icacos watershed (Puerto Rico). Geochim Cosmochim Acta 100: 73-95.

CHAPMAN RW & GREENFIELD MA. 1949. Spheroidal weathering of igneous rocks. Am J Sci 247: 407-429.

COELHO NETTO AL, SATO AM, AVELAR AS, VIANNA LGG, ARAÚJO IS, FERREIRA DLC, LIMA PH, SILVA AP & SILVA RP. 2011. January 2011: the extreme landslide disaster in Brazil. In: World Landslide Forum, 2, Roma, Proceedings... Roma: International Programme on Landslides (IPL), CD Rom, 6 p.

COLIN F, ALARÇON C & VIEILLARD P. 1993. Zircon: an immobile index in soils? Chem Geol 107: 273-276.

CONQ M, SILVEIRA CS & DOURADO F. 2015. Processos geomorfológicos e danos derivados da corrida de detritos de janeiro 2011 na bacia do Córrego do Príncipe, Teresópolis – Região Serrana do Rio de Janeiro. Ciência e Natura 37: 93-103.

EHLEN J. 2005. Above the weathering front: contrasting approaches to the study and classification of weathered mantle Geomorphology 67: 7-21.

FLETCHER RC, BUSS HL & BRANTLEY SL. 2006. A spheroidal weathering model coupling porewater chemistry to soil thicknesses during steady-state denudation EPSL 244: 444-457.

FRAIFELD F & FREITAS MM. 2013. Considerações geomorfológicas a respeito da corrida de massa do rio Vieira, Teresópolis – RJ. GeoPUC 10: 1-16.

GONÇALVES UG & FRANCISCO CN. 2016. Análise espacial das variáveis geomorfométricas e movimentos de massa na região serrana fluminense. RBC 68: 9.

GOUVEIA MI, FIGUEIREDO LCJ, PENA A, PEREIRA JC, PRUDENCIO MJ & WAERENBORG J. 1993. Behaviour of REE and other trace and major elements during weathering of granitic rocks, Evora, Portugal. Chem Geol 107: 293-296.

HALL K, THORN C & SUMNER P. 2012. On the persistence of 'weathering. Geomorphology 149/150: 1-10.

HEILBRON M, RIBEIRO A, VALERIANO CM, PACIULLO FV, ALMEIDA JCH, TROUW RJA, TUPINAMBÁ M & EIRADO SILVA LG. 2017. The Ribeira Belt. In: Heilbron M, Cordani U & Alkmim F (Eds), São Francisco Craton, Eastern Brazil. Regional Geology Reviews. Springer, Cham Eastern Brazil, p. 277-302.

LEBEDEVA MI, FLETCHER RC, BALASHOV VN & BRANTLEY SL. 2007. A reactive diffusion model describing transformation of bedrock to saprolite. Chem Geol 244: 624-645.

LI YHM, ZHAO WW & ZHOU MF. 2017. Nature of parent rocks, mineralization styles and ore genesis of regolith-hosted

REE deposits in South China: An integrated genetic model. J Asian Earth Sci 148: 65-95.

MARQUES AC, MATTOS CRC & SILVEIRA CS. 2017. Comportamento Hidrológico da Região Serrana do Rio de Janeiro: Bacia do Rio Piabanha. Anu do Inst de Geocienc 40: 82-88.

MIDDELBURG JJ, VAN DER WEIJDEN CH & WOITTIEZ JRW. 1988. Chemical processes affecting the mobility of major, minor and trace elements during weathering of granitic rocks. Chem Geol 68: 253-273.

MURAKAMI T, OHNUKI T, ISOBE H & SATO T. 1997. Mobitity of uranium during weathering. Am Min 82: 888-899.

NESBITT HW & MARKOVICS G. 1997. Weathering of the Toorongo Granodiorite, storage of elements in weathering profiles, and genesis of siliciclastic sediments. Geochim Cosmochim Acta 61: 1653-1670.

NESBITT HW, MARKOVICS G & PRICE RC. 1980. Chemical processes affecting alkalis and alkaline earths during continental weathering. Geochim Cosmochim Acta 44: 1659-1666.

NESBITT HW & YOUNG GM. 1982. Early Proterozoic climates and plate motions inferred from major element chemistry of lutites. Nature 299: 715-717.

OLLIER CD. 1971. Causes of spheroidal weathering. Earth Sci Rev 7: 127-141.

PRUDÊNCIO MI, SEQUEIRA BRAGA MAS & GOUVEIA MA. 1993. *REE* mobilization, fractionation and precipitation during weathering of basalts. Chem Geol 107: 251-254.

RODRIGUES J, TUPINAMBA M & AMARAL CP. 2013. A corrida de massa do rio Vieira em Teresópolis, sudeste do Brasil: caracterização da área-fonte dos sedimentos transportados. Anu do Inst de Geocienc 35: 152-164.

ROYNE A, JAMTVEIT B, MATHIESEN J & MALTHE-SØRENSSEN A. 2008. Controls on rock weathering rates by reaction-induced hierarchical fracturing. EPSL 275: 364-369.

SHUZUI H. 2001. Process of slip-surface development and formation of slip-surface caly in landslides in Tertiary volcanic rock, Japan. Eng Geol 61: 199-219.

SILVA CMCAC, BARBOSA RS, NASCIMENTO CWA & SILVA YJAB. 2018. Geochemistry and spatial variability of rare earth elements in soils under different geological and climate patterns of the Brazilian Northeast. Rev Bras Cienc Solo 42: e0170342.

STALLARD RF. 1985. River chemistry, geology, geomorphology, and soils in the Amazon and Orinoco basins. In: Drever JI (Ed), The chemistry of weathering, Rodez NATO, France, p. 293-316.

STALLARD RF. 1995. Tectonic, environmental, and human aspects of weathering and erosion: A global review using steady-state perspective. Annu Rev Earth Planet Sci 23: 11-39.

TAKENO N. 2005. Atlas of Eh-pH diagrams Intercomparison of thermodynamic databases Geological Survey of Japan Open File Report No. 419, 287 p.

TURKINGTON AV, PHILLIPS JD & CAMPBELL SW. 2005. Weathering and landscape evolution. Geomorphology 67: 1-6.

TURNER BF, STALLARD RF & BRANTLEY SL. 2003. Investigation of in situ weathering of quartz diorite bedrock in the Rio Icacos basin, Luquillo Experimental Forest, Puerto Rico. Chem Geol 202: 313-341.

VALVERDE MC & MARENGO JA. 2014. Extreme Rainfall Indices in the Hydrographic Basins of Brazil. OJMH 4: 10-26.

VELDE B & MEUNIER A. 2008. The Origin of Clay Minerals in Soils and Weathered Rocks. Berlin, Springer, Germany, 406 p.

WEN BP, DUZGOREN-AYDIN NS & AYDIN A. 2004. Geochemical characteristics of the slip zones of a landslide in granitic saprolite, Hong Kong: implications for their development and microenvironments. Environ Geol 47: 140-154.

WHITE AF, BLUM AE, SCHULZ MA, VIVIT DV, STONESTROM DA, LARSEN M, MURPHY SF & EBERL D. 1998. Chemical weathering in a tropical watershed, Luquillo Mountains, Puerto Rico: I. Long-term versus short-term weathering fluxes. Geochim Cosmochim Acta 62: 209-226.

WHITE AF, BLUM AE, SCHULZ MS, BULLEN TD, HARDEN JW & PETERSON ML. 1996. Chemical weathering rates of a soil chronosequence on granitic alluvium: I. Quantification of mineralogical and surface area changes and calculation of primary silicate reaction rates. Geochim Cosmochim Acta 60: 2533-2550.

YUSOFF ZM, NGWENYA BT & PARSONS I. 2013. Mobility and fractionation of REEs during deep weathering of geochemically contrasting granites in a tropical setting, Malaysia. Chem Geol 349/350: 71-86.

How to cite

SILVEIRA CS, RODRIGUES JG, ARARIPE DR, BERNEDO AVB & MANTOVANO JL. 2022. Geochemistry of a spheroidal weathering profile in a tropical mountainous landscape, Rio de Janeiro, Brazil. An Acad Bras Cienc 94: e20210544. DOI 10.1590/0001-3765202220210544.

Manuscript received on April 10, 2021;
accepted for publication on January 30, 2022

CARLA S. SILVEIRA[1]
https://orcid.org/0000-0002-1546-4719

JULIANA G. RODRIGUES[1]
https://orcid.org/0000-0002-5203-5323

DENISE R. ARARIPE[2]
https://orcid.org/0000-0002-7705-8310

ALFREDO V.B. BERNEDO[1]
https://orcid.org/0000-0003-3333-2565

JOSÉ L. MANTOVANO[3]
https://orcid.org/0000-0003-4931-2956

[1]Programa de Pós-Graduação em Geociências (Geoquímica), Universidade Federal Fluminense (UFF), Instituto de Química, Rua São João Batista, 2-188, Centro, 24020-141 Niterói, RJ, Brazil

[2]Universidade Federal Fluminense (UFF), Instituto de Química, Departamento de Química Analítica, Rua São João Batista, 2-188, Centro, 24020-141 Niterói, RJ, Brazil

[3] Instituto de Engenharia Nuclear (IEN/CNEN), Rua Hélio de Almeida, 75, Ilha do Fundão, 21941-614 Rio de Janeiro, RJ, Brazil

Correspondence to: **Carla Semiramis Silveira**
E-mail: carlasemiramis@id.uff.br

Author contributions

Carla S. Silveira: Conceptualization; Supervision, Writing original draft and review; Funding acquisition. Juliana G. Rodrigues: Formal analysis; Writing original draft. Denise R. Araripe: Supervision, Writing-Commentary. Alfredo V.B. Bernedo: Responsible for INAA analysis. José L. Mantovano: Responsible for XRF analysis.

CC BY